

# Delayed Babcock-Leighton dynamos in the diffusion-dominated regime

Y. Fournier, R. Arlt, and D. Elstner

Leibniz-Institut für Astrophysik Potsdam (AIP), An der Sternwarte 16, D-14482 Potsdam, Germany

Accepted . . . . Received . . . ; in original form . . .

## ABSTRACT

*Context.* Solar dynamo models of Babcock-Leighton type typically assume the rise of magnetic flux tubes to be instantaneous. Solutions with high-magnetic-diffusivity have too short periods and a wrong migration of their active belts. Only the low-diffusivity regime with advective meridional flows is usually considered.

*Aims.* In the present paper we discuss these assumptions and applied a time delay in the source term of the azimuthally averaged induction equation. This delay is set to be the rise time of magnetic flux tubes which supposedly form at the tachocline. We study the effect of the delay, which adds to the spacial non-locality a non-linear temporal one, in the advective but particularly in the diffusive regime.

*Methods.* Fournier et al. (2017) obtained the rise time according to stellar parameters such as rotation, and the magnetic field strength at the bottom of the convection zone. These results allowed us to constrain the delay in the mean-field model used in a parameter study.

*Results.* We identify an unknown family of solutions. These solutions self-quench, and exhibit longer periods than their non-delayed counterparts. Additionally, we demonstrate that the non-linear delay is responsible for the recover of the equatorward migration of the active belts at high turbulent diffusivities.

*Conclusions.* By introducing a non-linear temporal non-locality (the delay) in a Babcock-Leighton dynamo model, we could obtain solutions quantitatively comparable to the solar butterfly diagram in the diffusion-dominated regime.

**Key words.** dynamo, diffusion, Sun: magnetic fields

## 1. Introduction

The magnetic solar cycle is attributed to a dynamo process in which motions of a conductive medium are leading to the continuous induction of magnetic fields. Those motions may arise from convection which becomes anisotropic in the presence of rotation and stratification and is approximatively described by the  $\alpha$ -effect (Krause & Raedler 1980), or from the rise of magnetic structures to the solar surface, again in the presence of rotation and stratification, leading to what is called the Babcock-Leighton effect (Leighton 1969). While there has been no derivation of this effect from first principles so far, the synergy with the meridional circulation in the convection zone may lead to a periodic magnetic field explaining the solar cycle satisfactorily.

Babcock-Leighton dynamo were shown to reproduce qualitatively the solar butterfly diagram only if the turbulent magnetic diffusivity in the bulk of the convection zone is less than  $10^{12}$  cm<sup>2</sup>/s, a regime often referred to as the advective regime, since the meridional circulation then determines the cycle period. In the diffusive regime, the cycle period varies with the turbulent magnetic diffusivity and can be reduced to the observed cycle length, but the propagation of the dynamo wave then follows the Parker-Yoshimura rule and is poleward at all latitudes (Yoshimura 1975).

A variety of Babcock-Leighton dynamos has been published during the last 25 years, exemplarily by Choudhuri et al. (1995), Dikpati & Charbonneau (1999), Küker et al. (2001), Chatterjee et al. (2004), Guerrero & de Gouveia Dal Pino (2007), and Sanchez et al. (2014) for kinematic models with stationary flows

and dynamo effect, Nandy & Choudhuri (2001) for a model with toroidal-field loss by buoyancy, as well as Kitchatinov & Olemskoy (2011) for a nonlocal  $\alpha$ -effect similar to the Babcock-Leighton effect. A non-kinematic simulation showing a solar-like butterfly diagram is the one by Rempel (2006) with a turbulent magnetic diffusivity rising from  $10^{10}$  cm<sup>2</sup>/s to  $10^{12}$  cm<sup>2</sup>/s in the convection zone. Beyond the Sun, and among others, Jouve et al. (2010a) studied the cycle period dependence of Babcock-Leighton dynamos on the stellar rotation rate. The variability of the solar cycle including grand minima has been addressed with Babcock-Leighton dynamos by, for example, Karak (2010) who varied the meridional circulation, Olemskoy & Kitchatinov (2013) who varied the strength of their nonlocal source term, and Inceoglu et al. (2017) who varied both the generation of the flows and the Babcock-Leighton effect in a non-kinematic setup. In all these attempts, however, the effect of the toroidal magnetic field in the interior of the convection zone on the poloidal-field generation at the surface is instantaneous. Note that this list of Babcock-Leighton type dynamo papers is far from complete.

In the present Paper, we are addressing the problem that the Babcock-Leighton effect is not only nonlocal in space, but also in time. Following the pioneering work by Jouve et al. (2010b), we take a further step toward a fully constrained Babcock-Leighton dynamo. Here we use the results of global numerical simulations of flux-tube rise to improve and actually constrain a Babcock-Leighton dynamo model.

The global numerical simulations by Fournier et al. (2017) have shown that the rise time of magnetic flux tubes is independent of the magnetic diffusion. We suggest to treat this inde-

pendence with a non-locality in space and time, by designing a Babcock-Leighton dynamo model which has a time delay in the source term.

Non-localities have been shown to generate long-term variability in the amplitude and in the period of the magnetic cycle for a wide variety of models. A remarkable early attempt is the one by Yoshimura (1978) who used already a two-dimensional setup with source terms nonlocal both in space and time, delivering cyclic magnetic fields interrupted by “low-activity” periods of a few cycles duration. A sequence of papers on a zero-dimensional model, i.e. without any spatial dependence but with time delay, was published by Wilmot-Smith et al. (2006), Hazra et al. (2014) (including stochastic variations in the Babcock-Leighton effect), and Tripathi et al. (2018), who found sub-critical dynamo action, hinting on what we are going to show in this Paper in a two-dimensional spherical shell with realistic solar differential rotation. This is in line with the result by Rheinhardt & Brandenburg (2012) who studied the memory effect in a turbulent- $\alpha$  dynamo and found a threshold for dynamo excitation which is lower than in the case of no memory effect. There is actually a variety of papers on non-localities in turbulent- $\alpha$  dynamos which we do not review here. Closest to our approach is the work by Jouve et al. (2010b) who made the time delay magnetic-field dependent. However the authors always found that the time correlations required to obtain solar-like variability were too long to agree with the model’s assumptions.

Here we study such non-local models with time delays depending on the magnetic field strength, where the dependence is derived from the flux-rise simulations by Fournier et al. (2017). Section 2 describes the equations used and Section 4 shows the general results of using a delay in the induction equation. We discuss the implications of the results in Section 6.

## 2. The model and the reference setup

We derive our model from Jouve et al. (2008), and like in Jouve et al. (2010b) we introduce a delay into the Babcock-Leighton source term of a mean-field dynamo. In the current work, we will present the results of a large parameter study of more than 2000 simulations, partly constrained thanks to the results of global numerical simulations.

The model used here is simplified: we assume a constant turbulent magnetic diffusivity,  $\eta_t = \text{const}$ , in the stellar interior. Since the turbulent diffusivity is a measure of the turbulence intensity, a constant value implies that we can neglect radial turbulent pumping (Rädler 1968). This choice is made to prevent our setup from being polluted with weakly constrained parameters, namely an arbitrary profile of the magnetic diffusivity. Indeed, observations of decaying active regions suggest that the turbulent magnetic diffusivity,  $\eta_t$ , at the surface is of the order of  $10^{12} \text{cm}^2/\text{s}$ , while the mixing length theory provides an upper limit of  $10^{14} \text{cm}^2/\text{s}$  at the surface and  $10^{13} \text{cm}^2/\text{s}$  at the bottom of the convection zone. The large discrepancy between the various available estimates demonstrates the limit of our current knowledge. Additionally a constant turbulent magnetic diffusivity has the appreciable side effect that the Reynolds number is small everywhere allowing coarser grids and shorter computation times, which is adequate for a large parameter study.

Lengths and time are normalized with the stellar radius,  $R_\star$ , and the turbulent magnetic diffusion time,  $\tau_{\text{diff}} = R_\star^2/\eta_t$ . While the free choice of the unit of the magnetic flux density  $\mathbf{B}$  is made by setting the equipartition value with convective motions  $u_{\text{rms}}$  at  $r = 0.71$ ,  $B_{\text{eq}} = u_{\text{rms}} \sqrt{\mu_0 \rho}$  to unity, where  $\rho$  and  $\mu_0$  are the gas density and the permeability constant, respectively (see below).

The resulting dimensionless set of equations can be written in spherical coordinates  $(r, \theta, \phi)$  as:

$$\begin{aligned} \partial_t B_\phi &= \left( \nabla^2 - \frac{1}{\varpi^2} \right) B_\phi \\ &\quad - \text{Re} \varpi \mathbf{u}_p \cdot \nabla \left( \frac{B_\phi}{\varpi} \right) - \text{Re} (B_\phi \nabla) \cdot \mathbf{u}_p \\ &\quad + C_\Omega \varpi \left[ \nabla \times (\varpi A_\phi \mathbf{e}_\phi) \right] \cdot \nabla (\Omega), \\ \partial_t A_\phi &= \left( \nabla^2 - \frac{1}{\varpi^2} \right) A_\phi \\ &\quad - \text{Re} \frac{\mathbf{u}_p}{\varpi} \cdot \nabla (\varpi A_\phi) + C_S S, \end{aligned} \quad (1)$$

with  $B_\phi$ ,  $\mathbf{u}_p$ ,  $\varpi$ ,  $A_\phi$ ,  $\Omega$  and  $S$ , being the azimuthal magnetic flux density, the meridional circulation profile, the cylindrical distance to the rotation axis, the vector potential of the poloidal magnetic field, the angular velocity, and the source term for the poloidal field, respectively.

This system is controlled by three dimensionless parameters, the Reynolds numbers for the rotation and the meridional flow,  $C_\Omega$  and  $\text{Re}$ , and the dynamo number  $C_S$ .

$$\text{Re} = \frac{u_0 R_\star}{\eta_t}; \quad C_\Omega = \frac{\Omega_0 R_\star^2}{\eta_t}; \quad C_S = \frac{S_0 R_\star}{B_{\text{eq}} \eta_t}, \quad (2)$$

with  $u_0$ ,  $\Omega_0$ ,  $S_0$  being the maximum meridional velocity, angular velocity and Babcock-Leighton effect, respectively. The profile of  $\mathbf{u}_p$  and  $\Omega$  are normalized by  $u_0$  and  $\Omega_0$ , respectively.

The loose constraint on the amplitude and the profile of the meridional circulation gives some freedom for the choice of  $\text{Re}$ . The original model used a canonical profile aiming to catch the general characteristics of the solar flows. However the profile remained arbitrary, and the surface shear layer was missing. We suggest to take advantage of the results of Küker & Rüdiger (2011), where the authors provide consistent profiles of differential rotation and meridional flows based on the  $\Lambda$ -effect theory (Rüdiger 1989). This theoretical result provides a solar-like profile including a surface shear layer, with a single free coefficient, whose value is set to fit the helioseismic observations. The differential rotation and meridional circulation profiles and amplitudes are illustrated in Fig. 1.

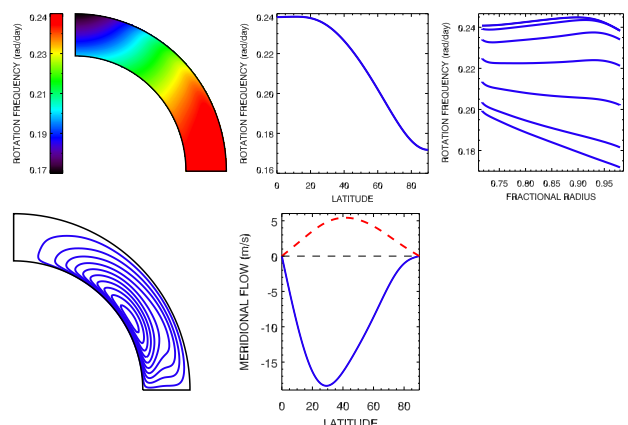


Fig. 1: Solar-like differential rotation and meridional circulation, obtained from a mean-field hydrodynamic simulation (Küker & Rüdiger 2011).

In Babcock-Leighton dynamos, the source term  $S$  is based on phenomenological arguments. Observations suggest that the

reversed polarity of the poloidal field emerging at the surface leads to a reversal of the large scale polar magnetic field. The source term  $S$  is an attempt to catch the physical processes behind the generation of poloidal field from the deeply seated toroidal field.

In the traditional frame of the Babcock-Leighton effect, for sufficiently large magnetic fields, buoyancy transports toroidal magnetic flux to the surface. During its rise through the convection zone, poloidal field can be generated under the action of the Coriolis effect, providing the necessary field at the surface for the Babcock-Leighton effect to work. Global simulations could show that buoyant magnetic structures locally quench the magnetic turbulent diffusivity,  $\eta_t$ , allowing them to remain coherent along their rise (Cattaneo & Hughes 1988). Additionally, Fan et al. (1994) showed that the solar meridional flow does not significantly affect the rise of magnetic flux tubes. Therefore, the buoyant transport of magnetic flux is independent of  $\eta_t$  and of the meridional flow,  $\mathbf{u}_p$ , and depends exclusively on the magnetic pressure, i.e. on  $B$ .

In the model presented here, we treat the transport's independence of  $\eta_t$  as a memory effect in the mean-field equations. The source of the poloidal field at the surface is correlated with the toroidal field at the bottom of the convection zone at an earlier time. The considered time correlation,  $\tau_{\text{delay}}$ , represents the time required by a buoyant magnetic structure to rise from the bottom of the convection zone to the surface.

We write the delayed source term as follow:

$$S(r, \theta, t) = f(r, \theta) \sum_{\tau_i} \left\{ \left[ 1 + \left( B_\phi(r_0, \theta, t - \tau_i) / B_{\text{quench}} \right)^2 \right]^{-1} B_\phi(r_0, \theta, t - \tau_i) \right\},$$

$$\text{for } B_\phi(r_0, \theta, t - \tau_i) > B_{\text{threshold}}, S = 0 \text{ otherwise.} \quad (3)$$

Where the sum is computed over all magnetic flux tubes reaching the surface at a given time  $t$ .

On the one hand, tubes with magnetic flux densities larger than  $B_{\text{quench}}$  are weakly affected by the Coriolis effect and emerge as untilted active regions (D'Silva & Choudhuri 1993; Jouve et al. 2013; Fournier et al. 2017). Such untilted regions do not provide poloidal magnetic flux to the Babcock-Leighton effect. On the other hand, weak flux tubes may be strongly affected by the turbulent convective motions such that they won't reach the surface. We consider a threshold,  $B_{\text{threshold}}$ , below which the toroidal field does not participate in the dynamo mechanism. Such a lower limit prevents the dynamo from growing from an arbitrarily low seed field.

Since the place where the source  $S$  operates remains unknown, we use the same arbitrary profile of Jouve et al. (2008), where  $S$  is nonzero at  $r \gtrsim 0.9$  and is maximum at  $45^\circ$  latitude at the surface.

$$f(r, \theta) = \frac{1}{2} \left[ 1 + \operatorname{erf} \left( \frac{r - 0.9}{0.02} \right) \right] \cos \theta \sin \theta. \quad (4)$$

### 2.1. Introducing the 3D results into the model

Thanks to global simulations it is now possible to constrain the correlation time,  $\tau_{\text{delay}}$ , the source-term quenching,  $B_{\text{quench}}$ , and the magnetic field threshold,  $B_{\text{threshold}}$ .

Here  $\tau_{\text{delay}}$  represents the rise time of magnetic flux tubes, i.e. coherent magnetic structures which may form from the destabilisation of a previously amplified magnetic layer (Rempel &

Schüssler 2001; Hotta et al. 2012), by the buoyancy instability (Parker 1955; Matthews et al. 1995; Wissink et al. 2000; Fan 2001; Kersalé et al. 2007; Favier et al. 2012). The amplification depends only on the stratification of the solar convection zone, and has been found to be  $F_{\text{amp}} = 10$  (Rempel & Schüssler 2001; Hotta et al. 2012). As a result amplified flux tubes can reach up to  $15 \cdot 10^4$  G (i.e.  $10 B_{\text{eq}}$ ).

Fournier et al. (2017) demonstrated that the rise time of magnetic flux tubes follows the relation:

$$\tau_{\text{delay}} \propto P_{\text{rot}} \left( \Gamma_{\alpha_1}^{\alpha_2} \right)^{\alpha_3}, \quad (5)$$

where  $P_{\text{rot}}$  is the rotation period of the star, and  $\Gamma_{\alpha_1}^{\alpha_2}$  is the ratio between the buoyant force and the Coriolis effect, modified by the magnetic tension. The exponent  $\alpha_3$  is a function of the azimuthal mode number with which the magnetic flux tube rises. In the case of the Sun, taking  $P_{\text{rot}}$  constant, this relation can reduce to:

$$\tau_{\text{delay}} \propto \tau_0 \left| \frac{B_\phi}{B_{\text{eq}}} \right|^\alpha, \quad (6)$$

with  $\alpha$  varying between  $-0.91$  and  $-2.0$  depending on the azimuthal mode. The parameter  $\tau_0$  is the rise time for a field in equipartition with the convective velocity,  $B_\phi = B_{\text{eq}}$  and is a free parameter. It depends on the rotation period of the star, the depth of its convection zone and the details of the destabilisation process forming the flux tubes as well as on the profiles of the turbulent thermal conductivity, viscosity and diffusivity. A discussion can be found in the Appendix.

In Eq. 6 there is no latitudinal dependence. But recalling that this equation describes the reduction of the rise velocity by the tension force we can model it following the latitudinal dependence of the tension force of  $1/\sin \theta$ .

$$\tau_{\text{delay}} = \frac{\tau_0}{\sin \theta} \left| \frac{B_\phi}{B_{\text{eq}}} \right|^\alpha. \quad (7)$$

We further define an effective delay  $\tau_{\text{eff}}$ , which turns out to be a very useful parameter. It corresponds to the shortest delay in any given moment, i.e.

$$\tau_{\text{eff}} = \tau_0 \left| \frac{B_\phi^{\text{max}}}{B_{\text{eq}}} \right|^\alpha, \quad (8)$$

where  $B_\phi^{\text{max}}$  is the strongest field strength generated by the  $\Omega$ -effect at the bottom of the convection zone. The maximum is taken over time and latitude (after saturation).

Rempel (2006) showed that Babcock-Leighton dynamos provide  $B_\phi$  up to  $3B_{\text{eq}}$ . Since the resulting amplified flux tubes are in the buoyancy dominated regime and therefore weakly participate in the dynamo because the Coriolis effect is not strong enough for significantly tilted active regions (see Appendix), we set  $B_{\text{quench}} = 3B_{\text{eq}}$ . Fan et al. (2003) have shown that amplified flux tubes weaker than  $3B_{\text{eq}}$  will not reach the surface as coherent structures. The lower threshold on  $B_\phi$  is  $B_{\text{threshold}} = 3B_{\text{eq}}/F_{\text{amp}} = 0.3B_{\text{eq}}$ . Since magnetic flux tubes of threshold flux density may have rise times of the order of  $t + 5\tau_{\text{diff}}$  for any moment  $t$  in the simulation, in order to prevent any issues with very long delays.

### 2.2. Behavior of the delay

The dependence of the delay on  $B_\phi$  is controlled by  $\alpha$ . When  $\alpha$  is set to zero, the delay is constant. A constantly delayed source

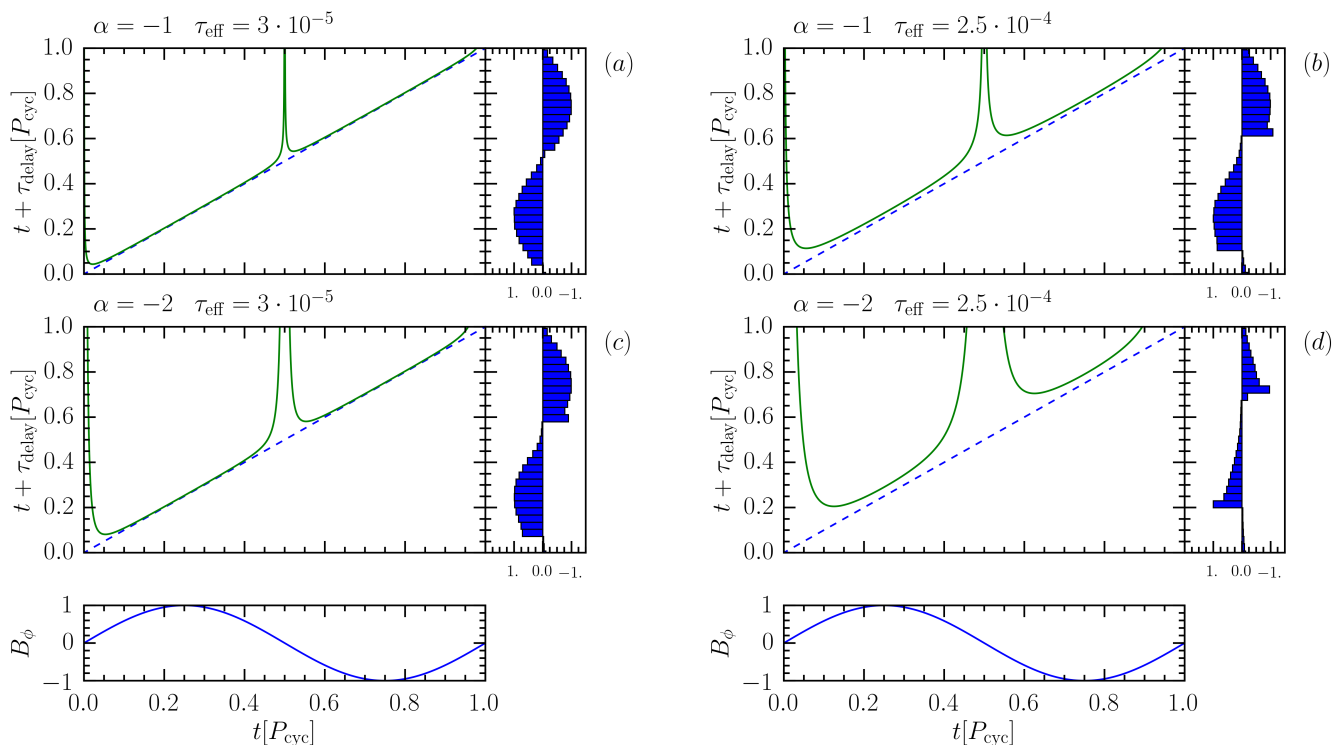


Fig. 2: Zero-dimensional toy model illustrating the effect of the delay. On each panel the green curve represents the evolution of the delay with time for a given  $B_\phi$ , indicated in the lower panel as the blue curve. The dashed line represents time. The histogram on the right-hand side represents the resulting source term  $S$  normalized in arbitrary unit. Panels (a) and (b), illustrate the case of a weakly non-linear delay ( $\alpha = -1$ ), whereas (c) and (d) a non-linear delay ( $\alpha = -2$ ). Panels (a) and (c) with a short effective delay (e.g.:  $B_\phi^{\max} = B_{\text{eq}}$  and  $\tau_0 = 3 \cdot 10^{-5} P_{\text{cyc}}$ ) and panels (b) and (d) with a long effective delay (e.g.  $B_\phi^{\max} = 0.5 B_{\text{eq}}$  and  $\tau_0 = 10^{-3} P_{\text{cyc}}$ ).

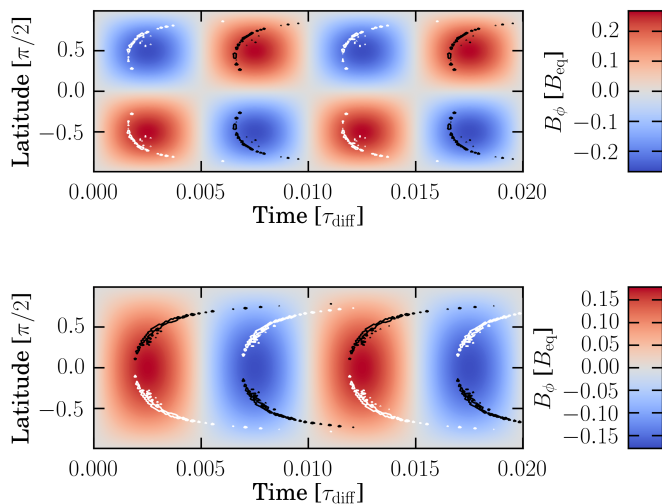


Fig. 3: Colour coding of the toroidal magnetic field strengths of an artificial oscillatory dipole (top) and an artificial oscillatory quadrupole (bottom). The contours represent the source term ( $S$ ) at the surface for  $\alpha = -2$  and  $\tau_0 = 10^{-2} P_{\text{cyc}}$ .

term has the same time-profile as a non-delayed source term, but is shifted in time. However as soon as  $\alpha$  becomes non-zero the delay becomes time-dependent. Weaker flux tubes rise longer than stronger ones. Weak flux tubes may therefore reach the surface at the same time than stronger flux tubes formed at a later

time. The time-dependence of the delay results into an accumulation of the source at the surface around certain times.

We illustrate this behavior in Fig. 2, for four different idealized cases. We consider a single point with a sinusoidally varying toroidal magnetic field,

$$B_\phi = B_\phi^{\max} \sin(\omega t) , \quad (9)$$

with amplitude  $B_\phi^{\max}$  and frequency  $\omega$ . The field is shown as blue curves in Fig. 2, while the red curves are the delay computed from  $B_\phi$ . The histograms show the resulting source of poloidal field accumulated from  $B_\phi$  in the past. Both upper panels show the case of a weakly non-linear, short- and a long- $\tau_{\text{eff}}$ , respectively (with  $\alpha = -1$ ). The two lower panels illustrate a strongly non-linear short- and long- $\tau_{\text{eff}}$  (with  $\alpha = -2$ ). In the weakly non-linear, short- $\tau_{\text{eff}}$  case the accumulation seen in the diagram is almost negligible and the time-profile of the source looks almost identical to the profile of  $B_\phi$ . It is only for a longer  $\tau_{\text{eff}}$  that the accumulation becomes visible. A similar accumulation is found for the non-linear, short- $\tau_{\text{eff}}$ , demonstrating that the non-linearity support the accumulation. In the case of the long- $\tau_{\text{eff}}$  the deformation of the profile leads to a “front”.

Clearly, there are two aspects of the delay which lead to accumulation, the length of the effective delay,  $\tau_{\text{eff}}$ , controlled by  $\tau_0$  and  $B_\phi^{\max}$ , and its non-linearity, controlled by  $\alpha$ .

Because of the latitudinal dependence of the toroidal magnetic field, the delay naturally varies with latitude. Like its time dependence, the latitudinal dependence of the delay is a function of  $\alpha$  and  $\tau_0$ , but it additionally depends on the sign of the latitudinal gradient of the toroidal field,  $\partial B_\phi / \partial \theta$ . As it can be seen in Fig. 3, if the toroidal field decreases toward the equator, the re-

sulting delayed field – illustrated by the contour plots – migrates equatorward, whereas when the gradient is directed poleward the dynamo wave propagates poleward. This is due to the fact that weaker fields are rising on a longer time scale and the accumulation is retarded setting the direction of propagation with the latitudinal gradient of  $B_\phi$ .

### 3. The non-delayed model

We solve Eqs. 1 with the pseudo-spectral, spherical code by Hollerbach (2000), in which the diffusion term is solved in spectral space, while the induction term is solved in real space. We do not employ the momentum and temperature equations of the code here. The induction equation solution took part in the benchmark by Jouve et al. (2008), and after implementing the delay term for the present study, we confirmed their results for  $\tau_{\text{delay}} = 0$  as is shown in Fig. 4. Our constant turbulent diffusivity of  $\eta_t = 10^{11} \text{ cm}^2/\text{s}$  as compared to the radius-dependent one in the benchmark, and our theory-based differential rotation versus the closed approximation in the benchmark do not modify the overall picture of the solutions. The slight difference in the amplitude of the meridional flow, due to the theoretical profile, explains the longer magnetic cycle of 40 yr compared to 30 yr of Jouve et al. (2010b). The solution is antisymmetric and oscillatory, with concentrated strong polar regions, and rather weak magnetic fields at low latitudes which are about  $10^{-3}$  of the high-latitude fields, migrating equatorward. The model is labelled as ADV in Tab. 1 and falls short of producing strong enough low-latitude toroidal fields for a realistic solar butterfly diagram. Another issue is the cycle which remains too long.

This solution is located in the advection dominated regime, where the magnetic cycle depends mostly on the meridional circulation. The meridional circulation amplitude is defined as a byproduct of the  $\Lambda$ -effect reproducing the solar differential rotation requiring only the mixing length parameter  $\alpha_{\text{MLT}}$ , so the only possibility to decrease the magnetic cycle in this setup is to increase the turbulent magnetic diffusion toward the diffusion dominated regime.

It is well known that dynamo solutions in the advection dominated regime differ from the ones in the diffusion dominated regime. On the lower panel of Fig. 4, we show a model in the diffusion dominated regime, with  $\eta_t = 10^{12} \text{ cm}^2/\text{s}$ . The relevant parameters can be found in Tab. 1 under the label DIFF. The solution remains antisymmetric and oscillatory, with an activity cycle period of 8 yr. The polar regions are less concentrated, closer to the solar characteristics and the low latitudes exhibit stronger fields ( $\approx 10\%$  of the high-latitude fields), but the dynamo wave propagates purely radially, as predicted by the Parker-Yoshimura rule.

Even if an  $\eta_t$  exists for which the non-delayed model gives a solution with an 11-year cycle period, the low latitude radial fields remain too weak as compared to the polar regions and the migration becomes radial while moving to the diffusion dominated regime.

### 4. Recovering the solar characteristics with the delay model

We model the rise time as a temporal non-locality, the delay, because Fournier et al. (2017) have shown in global simulations of rising magnetic flux tubes that the rise time is independent of the turbulent magnetic diffusion. In paragraph 2.2 we have shown that a time-dependent delay leads to temporal peaks in

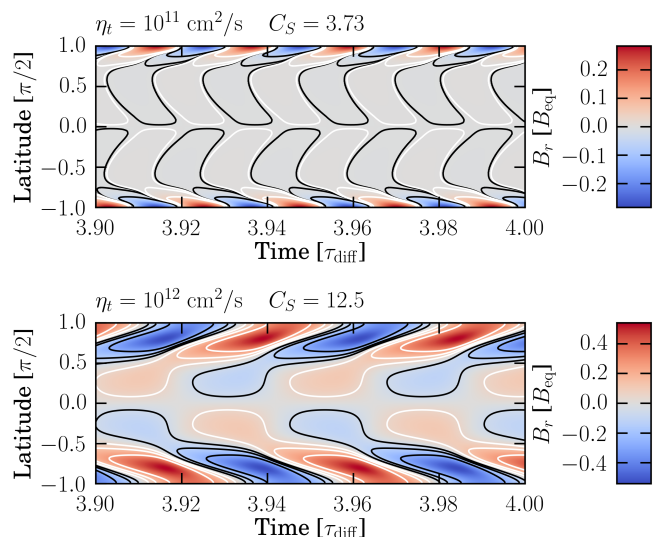


Fig. 4: Radial magnetic field at the surface as a function of time from the solutions in the advection dominated regime (ADV, top) and the diffusion dominated regime (DIFF, bottom). Contours also represent  $B_r$ , but show the 15, 1.5 and 0.15% levels of  $B_r^{\text{max}}$  for the top panel (ADV) and the 50, 25 and 10% levels of  $B_r^{\text{max}}$  for the bottom panel (DIFF). The parameters are summarized in Tab. 1.

the source term  $S$  of the induction equation near the surface, migrating latitudinally in the direction of decreasing toroidal field. We show below that the solar characteristics can only be recovered in the diffusive regime (model D-DIFF). We present one series of simulations in the advection dominated regime (D-ADV) and another one in the diffusion dominated regime (D-DIFF). In both series,  $C_S$  and  $\tau_0$  are varied. Since we found that the accumulation is largest in the nonlinear regime, we present two series with  $\alpha = -2$ . The parameters  $\text{Re}$  and  $C_\Omega$  are both fixed by the differential rotation profile, whose shape is determined by the  $\Lambda$ -effect and a standard solar model.  $B_{\text{quench}}$  and  $B_{\text{threshold}}$  are both constrained by the results of Fournier et al. (2017) and  $F_{\text{amp}}$  by Hotta et al. (2012). The two remaining parameters are  $C_S$  and  $\tau_0$ . Both are not yet constrained by any global simulation results. We have seen that  $\tau_0$  may determine the variability of  $S$  and  $C_S$  its amplitude. The parameters are summarized in Tab. 1.

#### 4.1. The advection dominated case

In this section we consider the ADV setup, in the advection dominated regime, with  $\eta_t = 10^{11} \text{ cm}^2/\text{s}$ . On the left panel of Fig. 5, we illustrate the maximum of the toroidal magnetic field at the bottom of the convection zone,  $B_\phi^{\text{cz}}$ , against  $C_S$ . The non-delayed series with  $\tau_0 = 0$  shows a critical source term amplitude of  $C_{S0}^{\text{crit}} = 3.534$  below which the model produces decaying solutions. It is remarkable that delayed dynamos deliver non-decaying solutions for weaker  $C_S$  than  $C_{S0}^{\text{crit}}$ . The delay has the surprising effect of reducing the criticality of the dynamo, opening a window to unknown solutions.

These solutions have the particular property to self-saturate at low amplitudes. The non-linearity of the delay acts as a quenching mechanism, which is appealing since the solutions become independent of the model used for the quenching.

The middle panel of Fig. 5 illustrates the dependence of the relative effective delay ( $\tau_{\text{eff}}/P_{\text{cyc}}$ ) on  $\tau_0$  and  $C_S$ . From this figure we could identify two different regimes: the short- $\tau_{\text{eff}}$  and the long- $\tau_{\text{eff}}$  regime.

Table 1: parameters of the various setups.

Setup	$\Omega_0$ [s <sup>-1</sup> ]	$u_0$ [m/s]	$\eta_t$ [cm <sup>2</sup> /s]	$C_\Omega$	Re	$C_S$	$\tau_0$ [ $\tau_{\text{diff}}$ ]	$B_{\text{quench}}$ [ $B_{\text{eq}}$ ]	$B_{\text{threshold}}$ [ $B_{\text{eq}}$ ]	$F_{\text{amp}}$
ADV	$2.68 \cdot 10^{-6}$	14.37	$10^{11}$	$1.3 \cdot 10^5$	1000	3.73	0.	32	0.1	10.
DIFF	$2.68 \cdot 10^{-6}$	14.37	$10^{12}$	$1.3 \cdot 10^4$	100	12.5	0.	32	0.1	10.
D-ADV	$2.68 \cdot 10^{-6}$	14.37	$10^{11}$	$1.3 \cdot 10^5$	1000	varied	varied	32	0.1	10.
D-DIFF	$2.68 \cdot 10^{-6}$	14.37	$10^{12}$	$1.3 \cdot 10^4$	100	varied	varied	32	0.1	10.
SOLAR	$2.68 \cdot 10^{-6}$	14.45	$6.7 \cdot 10^{11}$	$1.95 \cdot 10^4$	150	5.18	$10^{-3}$	32	0.1	10.

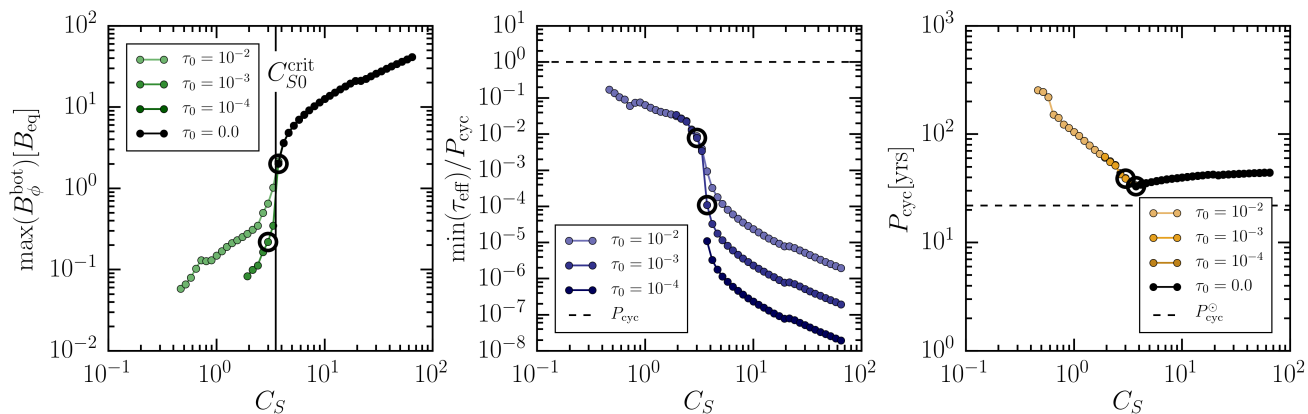


Fig. 5: D-ADV case. Saturation field strength (left), the effective delay (middle), and the cycle period (right), as functions of the source term amplitude  $C_S$  for four different delays. Each line represents a series of runs for a given delay. The vertical solid line marks the critical  $C_{S0}^{\text{crit}}$  for the non-delayed case. The circles identify the solutions shown in Fig. 6 .

In the short  $\tau_{\text{eff}}$  regime, the effective delay is several orders of magnitude shorter than the cycle period, and therefore produces almost identical solutions to the non-delayed case. Some accumulation is visible at mid-cycle (compare top panels of Fig. 4 and Fig. 6), for strongly non-linear delays ( $\alpha = -2$ ) but disappears for weaker non-linearity with  $\alpha = -1$ . The cycle period is independent of  $C_S$  as also shown in Fig. 5.

The second regime we identify is the long- $\tau_{\text{eff}}$  regime which is characterized by  $\tau_{\text{eff}}$  between  $10^{-3}P_{\text{cyc}}$  and  $10^{-1}P_{\text{cyc}}$ . This domain corresponds to the delay expected in the solar case – between a few days and a few months – and is therefore the regime of interest. The solutions self-saturate leading to a strong dependence of the saturation field and of the cycle period on  $C_S$ . The cycle period is also shown to be an increasing function of  $\tau_{\text{eff}}$ .

It appears that the transient peaks in  $S$  at the surface provide a sufficient source to maintain a dynamo which would otherwise decay. Therefore the saturation mechanism is not the quenching of the source term but the balance between the diffusion and the regular peaks of accumulated source term  $S$ . We still do not understand why an increase of the effective delay (lower  $C_S$ ) increases the cycle period.

Jouve et al. (2010b) studied the effect of  $\tau_0$  for a given  $C_S = C_{S0}^{\text{crit}}$ . Here we demonstrate that the delay reduces  $C_S^{\text{crit}}$  and identify two regimes. We studied the effect of  $\tau_0$  for each regime and extended the analysis of Jouve et al. (2010b).

In Fig. 5, it is remarkable that the effective delay and the cycle period are independent of  $\tau_0$ . The long- $\tau_{\text{eff}}$  regime results from the non-linearity of the delay, controlled by  $\alpha$ . Fournier et al. (2017) showed that  $\alpha$  is a function of the azimuthal mode with which an unstable flux tube rises. Determining under which condition one or the other mode is preferred will provide solid input to constrain this parameter.

Fig. 6 illustrates the radial field at the surface in the long- and short- $\tau_{\text{eff}}$  regimes. In both regimes the morphological characteristics of the delayed dynamo resemble the non-delay case: at high latitudes the strong polar fields are concentrated close to the pole propagating poleward; at low latitude, the radial fields remain weak showing an equatorward propagation. Even though the accumulation in  $S$  increases the field strength at low latitudes, it remains two orders of magnitude weaker than the polar fields.

Additionally in the short- $\tau_{\text{eff}}$  regime, the cycle period remains exclusively controlled by the meridional circulation, like in the non-delayed solutions, but in the long- $\tau_{\text{eff}}$  regime, the cycle period clearly increases, with decreasing  $C_S$ .

We conclude that the non-linear delay does not affect the qualitative characteristics of the dynamo, but, by increasing the cycle period, renders it a worse quantitative result. We summarize the dynamo characteristics in table 2.

#### 4.2. The diffusion dominated case

Estimates of the turbulent magnetic diffusivity from observations and mixing length based stellar models suggest a value of larger than  $10^{12}\text{cm}^2/\text{s}$ . However as seen on the lower panel of Fig. 4 for the non-delayed case in the diffusive regime, even though the cycle period of about 8 yr fits the observations better, the low latitudes remain weakly active and the dynamo wave propagates radially. The fact that turbulent magnetic diffusivities of less than  $10^{12}\text{cm}^2/\text{s}$  are required in order to obtain an equatorward migration has been a long-standing issue in Babcock-Leighton dynamos.

In Section 2.2, we have shown that for a prescribed sinusoidal magnetic field, the maximum field propagates in the lati-

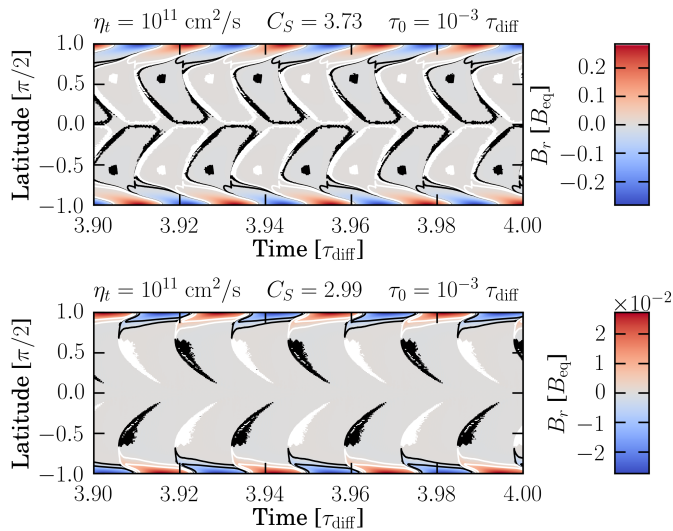


Fig. 6: Radial magnetic field at the surface as a function of time from the advection dominated case with delay (D-ADV) for two source term amplitudes  $C_S$ . The respective parameters are indicated above the plot. The black solid lines represent the 1.5 and 0.15% levels of  $B_r^{\max}$  for the short- $\tau_{\text{eff}}$  case (top), and the 25, 2.5% levels for the long- $\tau_{\text{eff}}$  case (bottom).

tudinal direction of the magnetic gradient, here we will discuss this mechanism for the simulated results.

As in the advection dominated regime, the introduction of the delay reduces the criticality of the dynamo, and opens a window towards new types of solutions. We could also identify the same regimes, illustrated in Fig. 7. The short- $\tau_{\text{eff}}$  regime remains identical to the non-delayed case, and suffers from the same differences to the solar cycle (see upper panel of Fig. 8). In the long- $\tau_{\text{eff}}$  regime the overall behavior is similar, the cycle period and the effective delay are independent of  $\tau_0$ . The solutions saturate before reaching  $B_{\text{quench}}$  (see left panel), and the cycle period decreases with  $C_S$  (see right panel). However, the morphologic characteristics of the dynamo are clearly different. On the lower panels of Fig. 8, we can see how the reduction of criticality allows an accumulation of  $B_r$  reaching  $\approx 25\%$  of the polar region’s field strength. Furthermore, the latitudinal distribution of the initial magnetic field (decreasing toward the equator) leads to an equatorward propagation in the low latitudes. The last panel of Fig. 8 shows a solution which quantitatively agrees with the solar characteristics (see table 2).

In this particular run  $\tau_{\text{eff}} = 3 \cdot 10^{-3} P_{\text{cyc}}$  which is about a few days. But solutions with effective delays up to a few months show comparable behaviors. So the non-locality introduces an additional time scale of the order of days which is sufficient to obtain accumulation of radial-flux generation at low latitudes and equatorward migration.

#### 4.3. Comparison to the solar case

The series we carried out in the diffusion dominated regime shows already a good quantitative agreement with the solar case, but we scanned the constrained parameter space with the remaining free parameters, namely  $\eta_t$ ,  $\tau_0$  and  $C_S$ , and selected a simulation, referred to as SOLAR, which reproduces the solar characteristics. Varying  $C_S$  and  $\eta_t$ , we could find a dynamo solutions whose butterfly diagram matches quantitatively several characteristics of the solar observations. We summarized these aspects

in Tab. 2. We have been comparing, the activity cycle period, the propagation of the active belt and of the high-latitude, the extent of the polar regions as well as the activity level of the low latitudes. We would like to remind the reader that the averaged strength of the observed active belts is about an order of magnitude weaker than the polar field strength.

The SOLAR solution is antisymmetric and oscillatory, with a cycle of 11 yr,  $36^\circ$  extent of the polar regions, with the amplitude of low latitudes being a fourth of the amplitudes of the polar regions, and an equatorward propagation of the active belt as well as a poleward propagation of the high-latitude fields. It is also remarkable that the polar reversal happens at half-cycle of the low latitude. The turbulent magnetic diffusivity required to obtain such a solution is  $\eta_t = 6.7 \cdot 10^{11} \text{ cm}^2/\text{s}$  which is in the transitional regime between the diffusive and the advective regime. The resulting effective delay  $\tau_{\text{eff}}$  is of the order of a month ( $\approx 33$  days). The toroidal field at the bottom of the convection zone saturates below equipartition with the convective motions, at about  $0.15 B_{\text{eq}}$ .

In Fig. 9, we illustrate various aspects of the dynamo mechanism showing how the toroidal field profile (a) is distorted into a source term sharply peaked in time (b), building up a “front” which, added to the diffuse field at the surface, leads to the very characteristics of the butterfly diagram (c). Because of the stiff accumulation, the active latitudes are strongly localized in latitude and time as compared to the solar butterfly diagram. As Weber et al. (2011) have shown that convective motions introduce stochasticity in the emergence characteristics of active regions, this mechanism could explain the broadening of the real solar activity bands in the butterfly diagram. We illustrate the propagation of the active latitudes in the meridional plane in Fig. 10 where the solid and dashed black contours represent the toroidal field, and the colour-coding shows the negative and positive radial field strength, respectively. The slices are taken in the beginning of the activity cycle, at maximum, in the decreasing phase and at minimum. The toroidal field peaks at high latitudes and propagates almost radially, as predicted by the Parker-Yoshimura rule. The strongest radial field is located at the pole. Close to the surface, where the source term is the strongest, the active latitudes, indicated by the dashed ovals, can be seen to migrate to the equator. These meridional sections demonstrate that the equatorward migration of the active belt does not follow the migration of the dynamo wave which propagates almost radially, but results from the longer delay for weaker toroidal fields closer to the equator.

## 5. Discussion of robustness of the results

Since some parameters remain weakly or even not constrained, it is important to discuss the robustness of the results of the previous Section.

The accumulation of the source term  $S$  in short-lived peaks due to the delay is the key aspect of the model which provides the solar-like characteristics. And for a prescribed oscillating magnetic field the accumulation is controlled by two parameters  $\tau_0$  and  $\alpha$  (see Section 2.2). Fournier et al. (2017) could constrain  $\alpha$  in the range of  $-0.91$  to  $-2$  depending on the unstable azimuthal mode of the rising flux tube. However one of the limitations of the latter work is the lack of constraint on  $\tau_0$ . It depends on many details of the formation of magnetic flux tubes and will be clearly challenging to constrain. Fortunately, we could demonstrate that the actual solutions in the long- $\tau_{\text{eff}}$  regime are clearly independent of  $\tau_0$ . As for the dependence on  $\alpha$  we have varied  $\alpha$  from  $-2$  to  $-0.1$  and found that solar-like solutions could be obtained

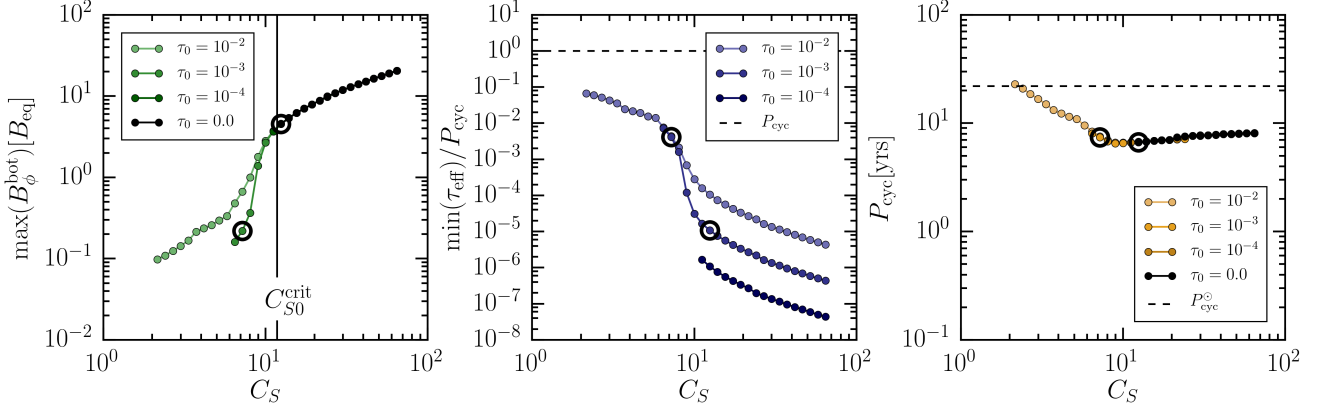


Fig. 7: D-DIFF case. Saturation field strength (left), the effective delay (middle), and the cycle period (right), as functions of the source term amplitude  $C_S$  for four different delays. Each line represents a series of runs for a given delay. The vertical solid line marks the critical  $C_{S0}^{\text{crit}}$  for the non-delayed case. The circles identify solutions shown in Fig. 8 .

Table 2: List of the characteristics of the dynamo, we have considered in this study.

	Obs./Est.	SOLAR	D-ADV	D-DIFF
$\eta_t$ [ $\text{cm}^2/\text{s}$ ]	$10^{10}-10^{14}$	$6.7 \cdot 10^{11}$	$10^{11}$	$10^{12}$
$P_{\text{cyc}}$ [yr]	11 (8–14)	$\approx 11$	30–300	6–20
low-latitude migration direction	equatorward	equatorward	equatorward	equatorward
high-latitude migration direction	poleward	poleward	poleward	poleward
polar-field cap extent	$35^\circ$	$36^\circ$	$9^\circ$	$45^\circ$
low latitudes	active	active	low activity	active

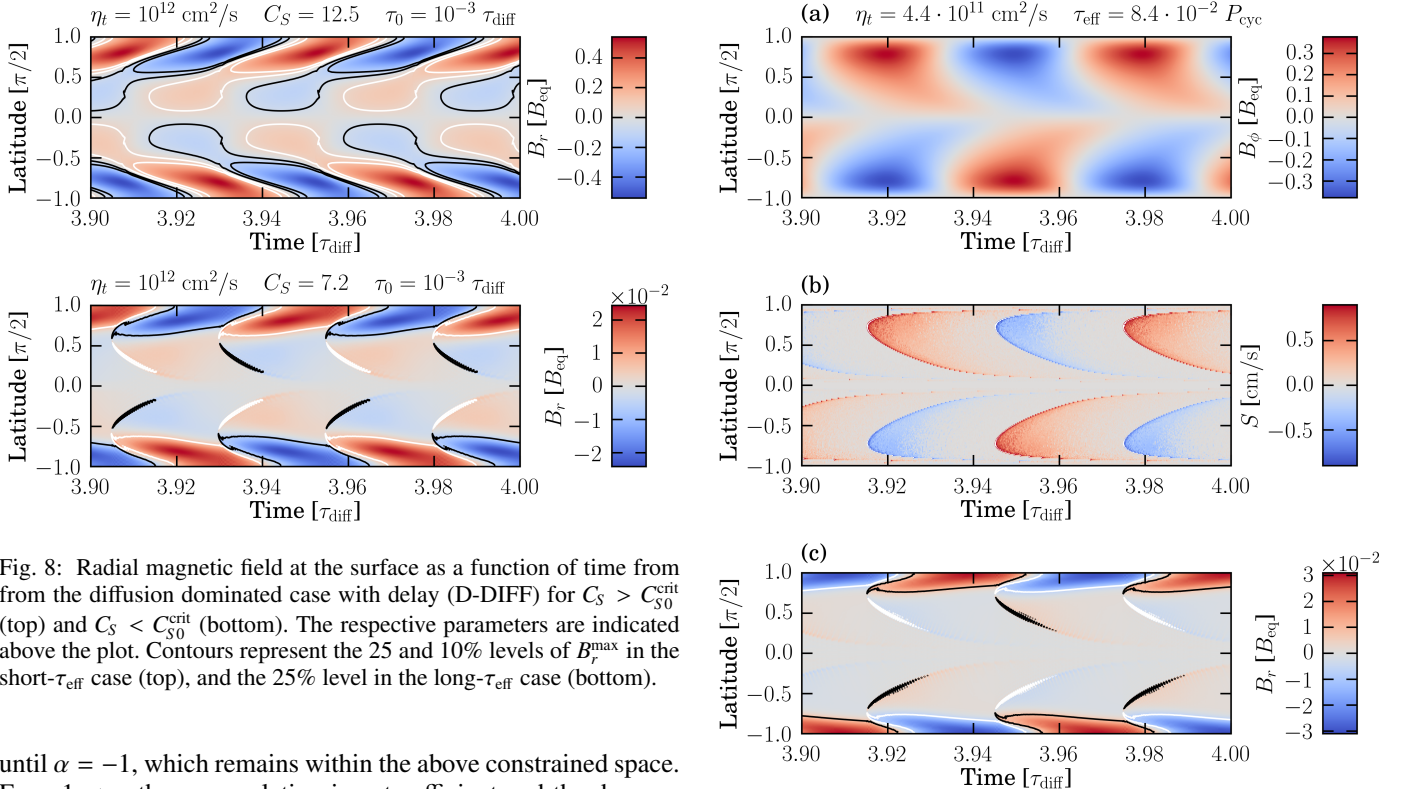


Fig. 8: Radial magnetic field at the surface as a function of time from from the diffusion dominated case with delay (D-DIFF) for  $C_S > C_{S0}^{\text{crit}}$  (top) and  $C_S < C_{S0}^{\text{crit}}$  (bottom). The respective parameters are indicated above the plot. Contours represent the 25 and 10% levels of  $B_r^{\text{max}}$  in the short- $\tau_{\text{eff}}$  case (top), and the 25% level in the long- $\tau_{\text{eff}}$  case (bottom).

until  $\alpha = -1$ , which remains within the above constrained space. For  $-1 < \alpha$  the accumulation is not sufficient and the dynamo decays.

Even though we could constrain the value of  $B_{\text{quench}}$  in the first term in the sum of (3), thanks to global numerical simulations, the quadratic quenching we use is quite arbitrary. But since this model possesses the surprising capability of self-quenching because of its non-linear non-locality, the solutions are indepen-

Fig. 9: Results of the SOLAR setup, with colour-coded toroidal magnetic field at the bottom of the convection zone (a), the resulting delayed source term at the surface (b) and the radial magnetic field at the surface (c). Contours in panel (c) represent the 25% level of  $B_r^{\text{max}}$ .

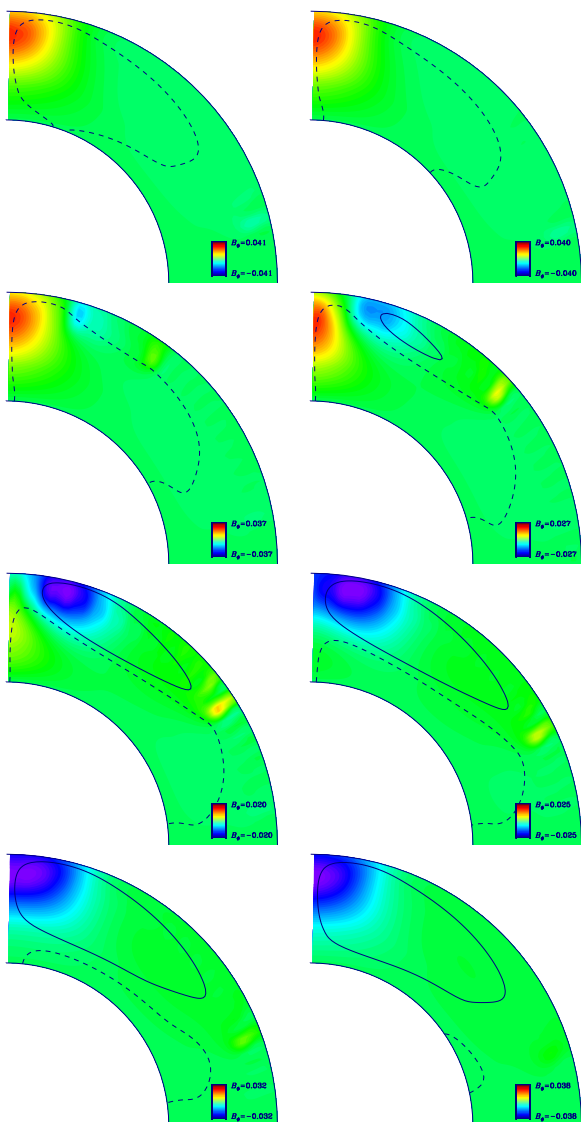


Fig. 10: Slices of the northern hemisphere. The slices are taken at different phases of the cycle, ordered from left to right and top to bottom: the rising phase, the maximum phase, the declining phase, and the minimum of the activity cycle. The colored contours represent the radial magnetic field, with red pointing outward and blue inward respectively. Contours are 5% and 2.5% of the maximum  $B_\phi$ .

dent of the chosen quenching model. The level of saturation only depends on the effective delay,  $\tau_{\text{eff}}$ , which is an outcome of the model and cannot be chosen arbitrarily.

Because we use a lower threshold on the magnetic field, some mode may not grow. The preferred mode of the dynamo is determined by the choice of the threshold and the initial condition. Although the threshold is relatively well constrained from the stability analysis of the buoyancy instability (Ferriz-Mas et al. 1994), it prevents the dynamo to grow from an arbitrary low seed field.

As is expected for the diffusion dominated regime, the cycle period depends on  $\eta_t$ , but in contrast to the non-delayed dynamos, the delayed model additionally shows a dependence on  $C_S$ . The cycle period may change by a factor of two over the relevant range of  $C_S$ . This is remarkable because it could explain how solar-like stars with a comparable rotation period and convective envelope (same  $\eta_t$ ) could show different magnetic cycles

– due to a difference in metallicity for instance. Such dependence needs to be carefully addressed because the interpretation of  $C_S$  as a physical quantity is not trivial. More global simulations will be required to be conclusive on this issue. But the non-local dynamos seems to be good candidates to address this particular issue.

## 6. Conclusions

Until now, diffusive Babcock-Leighton dynamos were considered not to be able to reproduce qualitatively the solar dynamo. The Parker-Yoshimura rule implies for the internal differential rotation of the Sun that the dynamo wave propagates poleward. We also find The cycle period to be too short as well as the low latitude radial fields to be too weak.

In the present work we introduced a delay in the source term of the poloidal field. Like in Jouve et al. (2010b), this delay represents the rise time of magnetic flux tubes through the convection zone. But in contrast to former studies, we built this model on the results of global numerical simulations of rising magnetic flux tubes in compressible stellar interiors (Fournier et al. 2017). The model consists of a rise time which depends nonlinearly on the magnetic flux density.

We have shown that the nonlinearity of the delay leads to an accumulation of the Babcock-Leighton source term at certain times. When this accumulation becomes sufficiently important, it may prevent the dynamo from decaying, even though the non-delayed model shows no dynamo action. The reduction of the criticality of the dynamo opens a new window to unknown solutions. These delayed dynamos have the peculiar property of self-quenching.

We found that the nonlinear delay can provide a mechanism to generate migration of the surface fields in the direction of weaker internal fields. In case of a stationary toroidal internal field at mid-latitudes, for example, the generated poloidal fields at the surface migrate towards the equator at low latitudes and towards the poles at high latitudes. This is independent of the sign of the internal differential rotation.

The requirement of a low turbulent magnetic diffusivity,  $\eta_t$ , for Babcock-Leighton dynamos to reproduce qualitatively the solar cycle, has been shown to be unnecessary. We demonstrate that the present delayed model, with a turbulent magnetic diffusivity of  $\eta_t = 6.7 \cdot 10^{11} \text{cm}^2/\text{s}$ , agrees well with the solar butterfly diagram, even though the diffusivity is relatively high throughout the entire convection zone.

Note that one proposed way out of the low-diffusivity problem is to use different values for  $\eta_t$  for the toroidal and for the poloidal components in the induction equation (Chatterjee et al. 2004). While the diffusivity may well be different in the horizontal and vertical directions, the poloidal field has varying components in both the horizontal and vertical directions, rendering the poloidal-field diffusivity location-dependent. We have not tried such a setup, and think it is actually not necessary given the results presented.

In any case, the model presented in this work is, by design, a simplified model. It has allowed us to identify the effect of the delay on the dynamo solutions. However several ingredients are missing to reach a state-of-the-art model (Rempel 2006; Cameron & Schüssler 2015; Pipin 2017). We only solve the induction equation for large-scale fields. We ignore the turbulent pumping, and the back-reaction of the magnetic field on the flow. All these elements will increase the complexity of the model and bring along additional free parameters which need to be constrained.

The large-scale field generation based on the Babcock-Leighton effect has not been derived from first principles. Its validity remains therefore uncertain. In the absence of global simulations addressing the formation of magnetic flux tubes, the current models remain quite arbitrary. Nevertheless, the non-linearities of the presented solutions are potentially relevant for other dynamos than the Babcock-Leighton type.

Finally, the relevance of this work for stellar dynamos will be revealed only if this model is proven to robustly reproduce observed dynamo patterns of further solar-like stars.

## 7. Acknowledgment

We would like to thank the participants and organizers of the Natural Dynamos (2016) conference for constructive remarks and input.

## References

- Cameron, R. & Schüssler, M. 2015, *Science*, 347, 1333  
 Cattaneo, F. & Hughes, D. W. 1988, *J. Fluid Mech.*, 196, 323  
 Chatterjee, P., Nandy, D., & Choudhuri, A. R. 2004, *A&A*, 427, 1019  
 Choudhuri, A. R., Schüssler, M., & Dikpati, M. 1995, *A&A*, 303, L29  
 Dikpati, M. & Charbonneau, P. 1999, *ApJ*, 518, 508  
 D’Silva, S. & Choudhuri, A. R. 1993, *A&A*, 272, 621  
 Fan, Y. 2001, *ApJ*, 546, 509  
 Fan, Y., Abbott, W. P., & Fisher, G. H. 2003, *ApJ*, 582, 1206  
 Fan, Y., Fisher, G. H., & McClymont, A. N. 1994, *ApJ*, 436, 907  
 Favier, B., Jouve, L., Edmunds, W., Silvers, L. J., & Proctor, M. R. E. 2012, *MNRAS*, 426, 3349  
 Ferriz-Mas, A., Schmitt, D., & Schuessler, M. 1994, *A&A*, 289, 949  
 Fournier, Y., Arlt, R., Ziegler, U., & Strassmeier, K. G. 2017, *A&A*, 607, A1  
 Guerrero, G. A. & de Gouveia Dal Pino, E. M. 2007, *Astronomische Nachrichten*, 328, 1122  
 Hazra, S., Passos, D., & Nandy, D. 2014, *ApJ*, 789, 5  
 Hollerbach, R. 2000, *Int. J. Numer. Meth. Fluids*, 32, 773  
 Hotta, H., Rempel, M., & Yokoyama, T. 2012, *ApJ*, 759, L24  
 Inceoglu, F., Arlt, R., & Rempel, M. 2017, *ApJ*, 848, 93  
 Jouve, L., Brown, B. P., & Brun, A. S. 2010a, *A&A*, 509, A32  
 Jouve, L., Brun, A. S., Arlt, R., et al. 2008, *A&A*, 483, 949  
 Jouve, L., Brun, A. S., & Aulanier, G. 2013, *ApJ*, 762, 4  
 Jouve, L., Proctor, M. R. E., & Lesur, G. 2010b, *A&A*, 519, A68  
 Karak, B. B. 2010, *ApJ*, 724, 1021  
 Kersalé, E., Hughes, D. W., & Tobias, S. M. 2007, *ApJ*, 663, L113  
 Kitchatinov, L. L. & Olemskoy, S. V. 2011, *Astronomische Nachrichten*, 332, 496  
 Krause, F. & Raedler, K.-H. 1980, *Mean-field magnetohydrodynamics and dynamo theory*  
 Küker, M., Rüdiger, G., & Schultz, M. 2001, *A&A*, 374, 301  
 Küker, M. & Rüdiger, G. 2011, *Astronomische Nachrichten*, 332, 933  
 Leighton, R. B. 1969, *ApJ*, 156, 1  
 Matthews, P. C., Hughes, D. W., & Proctor, M. R. E. 1995, *ApJ*, 448, 938  
 Nandy, D. & Choudhuri, A. R. 2001, *ApJ*, 551, 576  
 Olemskoy, S. V. & Kitchatinov, L. L. 2013, *ApJ*, 777, 71  
 Parker, E. N. 1955, *ApJ*, 121, 491  
 Pipin, V. V. 2017, *MNRAS*, 466, 3007  
 Rädler, K. H. 1968, *Zeitschrift f. Naturforschung Teil A*, 23, 1851  
 Rempel, M. 2006, *ApJ*, 647, 662  
 Rempel, M. & Schüssler, M. 2001, *ApJ*, 552, L171  
 Rheinhardt, M. & Brandenburg, A. 2012, *Astronomische Nachrichten*, 333, 71  
 Rüdiger, G. 1989, *Differential rotation and stellar convection. Sun and the solar stars*  
 Sanchez, S., Fournier, A., & Aubert, J. 2014, *ApJ*, 781, 8  
 Tripathi, B., Nandy, D., & Banerjee, S. 2018, *ArXiv e-prints* [arXiv:1804.11350]  
 Weber, M. A., Fan, Y., & Miesch, M. S. 2011, *ApJ*, 741, 11  
 Wilmot-Smith, A. L., Nandy, D., Hornig, G., & Martens, P. C. H. 2006, *ApJ*, 652, 696  
 Wissink, J. G., Hughes, D. W., Matthews, P. C., & Proctor, M. R. E. 2000, *MNRAS*, 318, 501  
 Yoshimura, H. 1975, *ApJ*, 201, 740  
 Yoshimura, H. 1978, *ApJ*, 226, 706

### Appendix A: Constraining $B_{\text{quench}}$ and $B_{\text{threshold}}$

The quenching field strength is defined such that the buoyant force balances the Coriolis force, resulting into a zero tilt at the surface. Fournier et al. (2017, Section 3) showed for the axisymmetric case that

$$\frac{F_{\text{buoy}}}{F_{\text{corio}}} = 0.7 \Gamma_1^1 \quad (\text{A.1})$$

with

$$\Gamma_1^1 = \frac{v_A}{\varpi \Omega} \quad (\text{A.2})$$

Presuming that the ratio of the buoyant force over the Coriolis force is unity for the quenching field strength, one obtains:

$$B_{\text{quench}} = \frac{1}{0.7} \varpi \Omega \sqrt{\rho \mu_0} = 32 \cdot 10^4 \text{G} = 32 B_{\text{eq}} \quad (\text{A.3})$$

with  $\Omega = 430 \text{ nHz}$ ,  $\rho = 0.1 \text{ g/cm}^3$ ,  $\varpi = 0.7 \cdot 2\pi \cdot 7 \cdot 10^{10} \text{ cm}$  and  $B_{\text{eq}} = \sqrt{\mu_0 \rho u_{\text{rms}}^2} = 10^4 \text{ G}$  with  $u_{\text{rms}} = 100 \text{ m/s}$ .

The field strength of a magnetic flux tube which reaches the surface needs to be larger than  $3B_{\text{eq}}$  (Fan et al. 2003). The threshold field strength is therefore  $3B_{\text{eq}}$ .